Xiaoxin Wang
Department of Aerospace and Mechanical Engineering,
The University of Arizona,
Tucson, AZ 85721
e-mail: wangxx850815@email.arizona.edu

Jesus Del Rincon
Department of Aerospace and Mechanical Engineering,
The University of Arizona,
Tucson, AZ 85721
e-mail: delrinconj@email.arizona.edu

Peiwen Li
Department of Aerospace and Mechanical Engineering,
The University of Arizona,
Tucson, AZ 85721
e-mail: peiwen@email.arizona.edu

Youyang Zhao
National Renewable Energy Laboratory,
15013 Denver West Parkway,
Golden, CO 80401
e-mail: youyang.zhao@nrel.gov

Judith Vidal
National Renewable Energy Laboratory,
15013 Denver West Parkway,
Golden, CO 80401
e-mail: judith.vidal@nrel.gov

Thermophysical Properties Experimentally Tested for NaCl-KCl-$MgCl_2$ Eutectic Molten Salt as a Next-Generation High-Temperature Heat Transfer Fluids in Concentrated Solar Power Systems

A new eutectic chloride molten salt, $MgCl_2$-KCl-NaCl (wt% 45.98–38.91–15.11), has been recognized as one of the most promising high-temperature heat transfer fluids (HTF) for both heat transfer and thermal storage for the third-generation concentrated solar power (CSP) systems. For the first time, some essential thermophysical properties of this eutectic chloride molten salt needed for basic heat transfer and energy storage analysis in the application of concentrating solar power systems have been experimentally tested and provided as functions of temperature in the range from 450 °C to 700 °C. The studied properties include heat capacity, melting point, heat of fusion, viscosity, vapor pressure, density, and thermal conductivity. The property equations provide essential database for engineers to use to calculate convective heat transfer in concentrated solar receivers, heat exchangers, and thermal storage for concentrated solar power plants.
[DOI: 10.1115/1.4049253]

Keywords: heat-transfer fluid, thermophysical properties, eutectic chloride molten salt, $MgCl_2$-KCl-NaCl, CSP, energy, heat transfer, materials, solar, testing

1 Introduction

As one of the major types of clean and renewable energy, solar energy attracts more and more attention for the modern society to meet the continuous and increasing demand of clean energy rather than the traditional fossil fuels [1–4]. The combustion of fossil fuels has the disadvantage of causing increased pollution of air and increased global warming due to Green-house effect [5,6]. Photovoltaic (PV) and concentrated solar power (CSP) are the two major solar energy technologies in the present time. Solar PV is the most fast-growing technology that converts energy from photons into electricity directly based on the photovoltaic effect [7]. However, the energy conversion efficiency of commercial PV is still relatively low and also providing electrical energy at nighttime or bad weather by PV systems is still restricted due to the difficulties and high cost of electrical energy storage [8]. As a very good complementary technology to the PV power generation, CSP has the advantages of higher solar-to-electrical energy conversion efficiency, and more importantly, its thermal storage capability allows the extended baseload power generation at night and bad weather conditions [9]. A CSP system can store a large quantity of solar thermal energy to meet a longer time of energy demand than just the period of daytime with sunlight.

To deliver the heat from a solar receiver to a heat exchanger and thermal storage tank, a fluid capable of operating at high temperature with desirable thermal and transport properties is needed for a CSP system. Such a fluid is often called as heat transfer fluid (HTF), but it is also required to be able to store thermal energy. This means that the HTF needs high density and heat capacity and also should have relatively low cost and large reserve available in nature. Low-cost heat-transfer fluids such as water [10], air [11], and supercritical CO_2 [12,13] cannot meet the requirement for energy storage at high temperatures. Materials like thermal conductive oils [14,15], molten salts, and liquid metals [16] have been screened comprehensively for HTF and thermal storage media. Thermal conductive oils could be used as HTF in commercial solar thermal power plants with relatively low solar concentration ratios and temperatures less than 400 °C [14,17]. For the most advanced CSP system, high energy conversion efficiency is a basic requirement, which needs high-temperature HTF and thermal storage media. Therefore, molten salts are generally recognized as feasible materials to satisfy operating temperatures higher than 400 °C. Composed of nitrate salts, $NaNO_3$ and KNO_3 in molar ratio of 60% versus 40%, solar salt has been successfully used for the working temperature ranges from 290 to 565 °C, which starts to decompose at temperatures beyond [18]. Alkali carbonate eutectic molten salt has also been studied to serve as HTF and thermal energy storage (TES) media by many researchers [19,20]. An et al. [21] provided thermophysical properties of eutectic carbonate salt Li_2CO_3-Na_2CO_3-K_2CO_3 in a weight ratio of 32.12–33.36–34.52% studied through experimental tests. This eutectic carbonate molten salt was found to be stable at a temperature below 658 °C and has promising thermal physical properties. However, the large demand and relative high cost of the component, Li_2CO_3, restricts the application of this eutectic carbonate salt in CSP.

In the recent few years, eutectic chloride salts including $MgCl_2$, KCl, and NaCl have received a significant attention in the CSP society, where efforts are focused on increasing operating temperatures up to 800 °C for high energy conversion efficiency, and at the

Contributed by the Solar Energy Division of ASME for publication in the Journal of Solar Energy Engineering: Including Wind Energy and Building Energy Conservation. Manuscript received July 21, 2020; final manuscript received November 16, 2020; published online January 11, 2021. Assoc. Editor: Wei Li.

same time to have reduced cost of thermal energy storage. These chloride salts have abundant reserve in nature and have relatively low cost. Low vapor pressure, good stability at temperatures up to 800 °C, and good material compatibility have been reported [22] about the binary eutectic salt of $MgCl_2$ and KCl.

In the recent time, a new eutectic chloride salt comprised $MgCl_2$-KCl-NaCl (at wt% of 45.98–38.91–15.11) was reported in Zhao and Vidal's work [23]. This ternary eutectic chloride salt has a melting point 40 °C lower than that of the binary chloride eutectic salt by $MgCl_2$ and KCl [22], which is an appreciable benefit regarding prevention of freezing of molten salt. Researchers at National Renewable Energy Laboratory of U.S. have developed processing technologies to obtain the designated eutectic compositions from natural mineral salts [23]. Whereas this ternary eutectic chloride salt is widely considered in the USA as the third-generation high-temperature heat transfer and thermal storage fluid in the community of CSP [23], there have no studies and report about its basic thermophysical properties.

To promote the understanding to this eutectic chloride salt $MgCl_2$-KCl-NaCl (at wt% of 45.98–38.91–15.11), the present study will take experimental measurement about the essential thermophysical properties for the first time in the world. These properties should include heat capacity, melting point, heat of fusion, viscosity, vapor pressure, density, and thermal conductivity, which are essentially needed for the calculation of convective heat transfer in concentrated solar receivers, heat exchangers, as well as thermal storage system for CSP plants.

2 Experimental Setups and Tests

2.1 Differential Scanning Calorimetry Measurement for Melting Point, Specific Heat Capacity, and Heat of Fusion. The eutectic chloride salt melting point, specific heat capacity, and heat of fusion were measured by using a simultaneous differential scanning calorimetry (DSC) and thermogravimetric analysis (TG) system (Model STA449 F3 made by NETZSCH). Argon is used as the protective gas. A great amount of effort has been made to calibrate the STA449 F3 system and ensure that repeatability of tested data is rigorously maintained [24]. The systematic error of the DSC signal is ±2% of reading; while the temperature measurement systematic error is 0.2 °C. It was interesting that the molten salt in graphite crucibles did not show creeping effect, which however is significant in platinum crucibles. Thus, crucibles made of high-density graphite were used in the test for specific heat capacity. ASTM [25] defined standard procedures and temperature increasing steps for measurement of specific heat capacity were followed in all the tests [26].

2.2 Measurement of Viscosity. The viscosity of high-temperature molten salt was measured using a high-temperature viscometer (Brookfield viscometer). The instrument is custom-designed and manufactured by Theta Industrials Inc. Rigorous calibration to the viscometer was conducted using Cannon Certified Viscosity Reference Standard Oil for comparison so that the system error is negligible. The instrument was also checked by measuring the viscosity of a eutectic molten salt, NaCl-KCl-$ZnCl_2$ (Mole: 20–20–60%), which has available viscosity data in literature [27]. In our previous work for the calibration measurement [28], it showed a deviation of less than ±2% between the measured mean data (from multiple tests) and reported data in literature. In the measurement to the eutectic $MgCl_2$-KCl-NaCl molten salt, three samples of the same compositions were prepared, and each of the sample was tested for two times. The repeatability of measured data was checked, which showed a deviation of the tested data from the tested mean data less than ±5% at any temperature point.

2.3 Vapor Pressure Test. The setup for high-temperature eutectic molten salt vapor pressure test is shown in Fig. 1 schematically. The salt is enclosed in a sealed quartz test tube. A small condenser with circulated airflow is placed right above the liquid salt surface to ensure that molten salt vapor is cooled into liquid and drops back to the bulk liquid, which thus prevents the large amount of salt vapor from solidifying in the tube or pressure transducer. A pair of K-type thermocouple protected by a thin quartz tube is put into the molten salt to measure temperature. The sealed quartz test tube is housed in a furnace (Bartlett, Model 3 K) to keep a desired stable temperature for the molten salt. A vacuum pump was used to make the absolute pressure inside the closed system to close to zero as much as possible at the beginning of the test. A pressure transducer with an accuracy of ±0.08% of reading and a full scale pressure of 50 psi (3.447×10^5 Pa) is connected to the test tube to measure the absolute pressure in the system. The pressure and temperature data are recorded by a

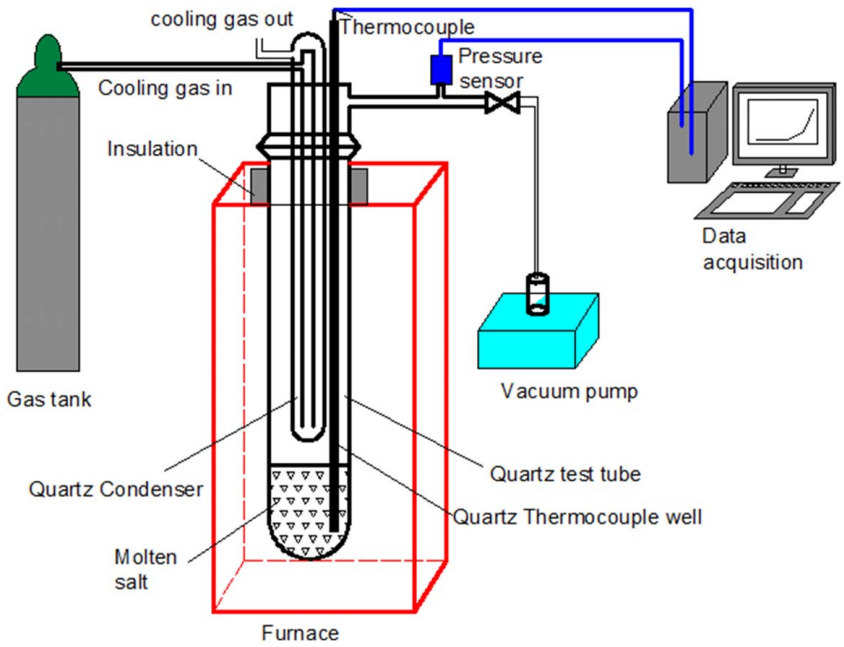

Fig. 1 Schematic of the setup of vapor pressure measurement [28]

LabVIEW supported data-acquisition system during the experiment. The reliability of this system was verified by Wang et al. in a previous work [28] in the authors' laboratory. In the calibration test [28], the vapor pressure of $ZnCl_2$ was measured using the system. The results of measured vapor pressure of $ZnCl_2$ were compared with literature-reported data, and a maximum discrepancy was found to be less than ±5 kPa, when the pressure is below 100 kPa. For a pressure as high as 1200 kPa, the maximum discrepancy could be as high as 120 kPa. The overall measured curve of the pressure versus temperature of the molten salt ($ZnCl_2$) from 400 K to 1200 K matched with literature-reported data very well.

2.4 Molten Salt Density Measurement. The density of molten salt was measured by an in-house-developed density meter designed based on Archimedes' principle on buoyancy. During the measurement, the weight of an object (high purity Nickel cylinder) was measured before and after submerging in the molten salt in a quartz container. A balance of systematic error of ±0.1% of full scale (50 g) was used to measure the masses. With the obtained difference of the mass of the object staying in air and in molten salt, the density of the molten salt at different temperatures can be calculated by the following equation:

$$\rho_f = \frac{\Delta M}{M} * \rho_M \tag{1}$$

where ΔM is the weight difference of the Nickel cylinder caused by the buoyancy force of the molten salt, M is the weight of the Nickel cylinder measured in the air, and ρ_M is the density of Nickel cylinder. The measurement system was calibrated in the previous work and the results showed good reliability and accuracy [29,30]. Based on the systematic error of the balance, the systematic error of measured density can be calculated referring to the basic equation (Eq. (1)) using partial derivative error propagation method.

2.5 Thermal Conductivity Obtained Through Measurement of Thermal Diffusivity, Density, and Specific Heat Capacity. The thermal conductivity of high-temperature molten salt is determined through Eq. (2)

$$k = \alpha * \rho * C_p \tag{2}$$

where ρ and C_p are density and the specific heat, respectively, which are experimentally measured through the facilities and approaches described in Secs. 2.1 and 2.4. The thermal diffusivity α was directly measured by using a Laser Flash Analysis equipment (Model LFA 457, MicroFlash, by NETZSCH), which can operate at a temperature as high as 1000 °C. The systematic error of the diffusivity measurement is ±3% of reading. The series of measured thermal diffusivity data was collected and recorded in the experiment. With the input of the separately tested density and heat capacity, the thermal conductivity is analyzed and calculated through the NETZSCH LFA supported software. The uncertainty of the thermal conductivity can be obtained using partial derivative error propagation method referring to Eq. (2) as the basic equation.

3 Experimental Data Reduction, Results and Discussion

3.1 Specific Heat Capacity, Melting Point, and Heat of Fusion. There were 18 measurements conducted for the specific heat capacity (C_p) of the molten salt at each temperature. These measurements were accomplished for a batch of six salt samples each tested for three times. Figure 2 shows the 18 curves for the tested specific heat capacity versus the temperatures. At every temperature point, there are 18 data of specific heat capacity. The mean value of the specific heat capacity (C_p) at every temperature point is calculated and uncertainty analysis was made for the measured mean value of specific heat capacity. The standard deviation and

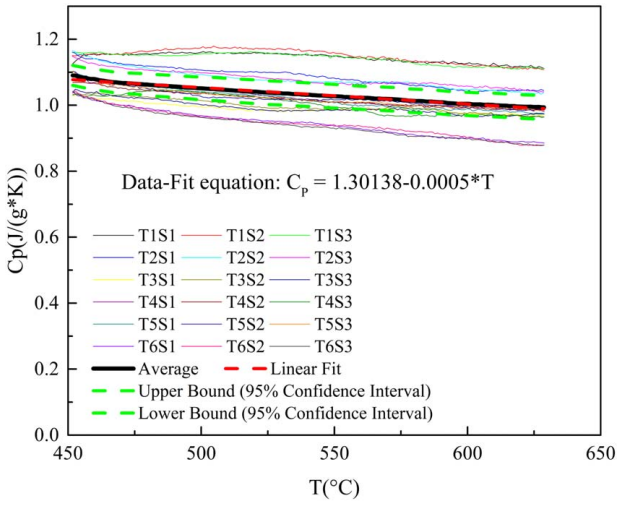

Fig. 2 Specific heat capacity versus the temperature for the molten salt

random error at a probability of 95% were obtained using Eqs. (3) and (4) for the experimental data

$$S_Y = \sqrt{\frac{\sum_{i=1}^{N}(Y_i - \bar{Y})^2}{N_1 - 1}} \tag{3}$$

$$u_1 = t_{\nu 1,95\%}\frac{S_Y}{\sqrt{N_1}} \tag{4}$$

$$u_{\bar{Y}} = \sqrt{u_1^2 + u_0^2} \tag{5}$$

where the term Y in Eq. (3) can represent a measured parameter at different temperatures, N_1 is the number of measurements, which is 18 in this case, t is the adopted student-t number for a confidence interval of 95% and degree of freedom, $\nu_1 = N_1 - 1$. Equation (5) gives the expression for measurement uncertainty, where u_1 is the random error and u_0 is systematic error. The calculated results at several chosen temperatures are shown in Table 1. The maximum measurement uncertainty entailing systematic error (±2% of reading) and random errors for the mean value of C_p is obtained as ±0.0358 J/g · K at a confidence interval of 95%.

The curve of the mean value of measured specific heat capacity at all the temperatures is shown in Fig. 2, which is used for regression analysis to determine the correlation of the specific heat capacity versus temperature. The regression equation in a linear form is given in Eq. (6) in the temperature range of 450–630 °C

$$C_p = 1.30138 - 0.0005 * T \tag{6}$$

where C_p is in the unit of J/g · K, and T is in °C. The uncertainty of curving fitting is calculated using Eq. (7)

$$u_c = t_{\nu_2,95\%}\frac{S_c}{\sqrt{N_2}} = t_{\nu_2,95\%}\sqrt{\frac{\sum_{i=1}^{N}(Y_i - Y_c)^2}{\nu_2 * N_2}} \tag{7}$$

Table 1 Measured average values and the overall uncertainty of specific heat capacity

T (°C)	450	500	550	600	628
$\overline{C_p}$ (J/g · K)	1.0904	1.0511	1.0271	1.004	0.9936
$u_{\overline{C_p}}$ (J/g · K)	0.0305	0.0348	0.0358	0.0351	0.0357

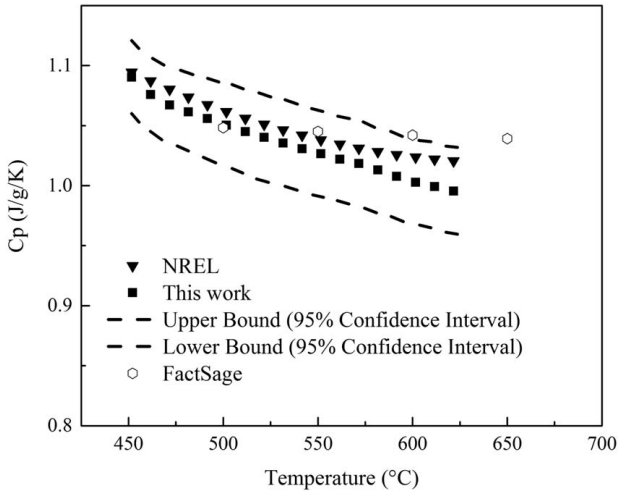

Fig. 3 Measured viscosities at various temperatures

where N_2 is the number of all the data for regression, S_c is the standard deviation between all the data from measurement and the calculated data using the regression equation, t is student-t number at 95% confidence interval, $v_2 = N_2 - (m+1)$, m is the order of polynomial curve fitting equation, Y_i is the measured data, Y_c is the calculated data from curve fitted equation. The overall uncertainty of the obtained correlation of $C_p - T$ is calculated through Eq. (8), which counts the uncertainty of measurement (systematic and random errors) and the uncertainty from data fitting

$$u_{total}^{max} = \sqrt{(u_{\overline{Y}}^{max})^2 + u_c^2} \tag{8}$$

The uncertainty from curve fitting is u_c (4.28×10^{-4} J/g · K), which is much less than the measurement uncertainty $u_{\overline{C_p}}$, and thus, the maximum overall uncertainty is still 0.0358 J/g · K.

As shown in Fig. 3, the regression equation of the measured mean specific heat capacity at the University of Arizona is compared with the measured data from another research team (authors at National Renewable Energy Laboratory (NREL)) and also with the data from theoretical prediction obtained using the software Factsage [31,32]. The relative difference between the measured mean values by the two teams is less than 5%. To minimize the random effect of experimental conditions, both of the two teams used the same procedure to measure the heat capacity of this ternary molten salt, including the same temperature program, type of graphite crucibles, protection gas, and flowrate. However, different models of the equipment of Differential Scanning Calorimetry (STA449 F3 versus DSC 404 F3 Pegasus both made by NETZSCH) were used by the two teams, the systematic error may cause the small discrepancy of the two group of data. A number of random factors can also affect the results in heat capacity measurement, which include errors due to positioning of crucibles in the sample holder, the magnitude of crucible surface oxidation that influences the radiation heat transfer in the test process, etc. Discussions about having a reliable measurement for heat capacity has been reported in another work by the author's team [29]. The current agreement of the measured data and the predicted data are also less than 5%, which is satisfactory. It is important to note that the heat capacity of the molten salt slightly decrease with the increase of temperature. This has been demonstrated from the experimental data as well as from the theoretical prediction.

The measured data for the melting point of the molten salt is given in Table 2, where there are 15 measurements. The mean value and the measurement uncertainty (including systematic error of 0.2 °C and random error) at a confidence interval of 95% for the melting point (T_m) of the molten salt are given in the table. The 15 data show the average melting point to be 401.4 °C, and the measurement uncertainty at a probability of 95% is ±1.3 °C.

Table 2 Measured average values and overall uncertainty of melting point

Test ID	1	2	3	4	5	6	7	8
T_m (°C)	401.3	401.4	396.8	407.4	399.3	399	400.9	401.2
Test ID	9	10	11	12	13	14	15	
T_m (°C)	401.5	401.8	406.8	400.3	400.8	401	401.5	
$\overline{T_m}$ (°C) = 401.4; $\overline{T_m}$ (°C) = ±1.3								

Table 3 Measured average values and overall uncertainty of heat of fusion

Test ID	1	2	3	4	5	6	7	8
ΔH (kJ/kg)	265.3	259.4	248.3	256.6	245	265.6	245.5	252.3
Test ID	9	10	11	12	13	14	15	
ΔH (kJ/kg)	246.4	239.3	257	252.5	236.5	224.6	230.5	
$\overline{\Delta H_m}$ (kJ/kg) = 248.32; $u_{\overline{\Delta H_m}}$ (kJ/kg) = ±7.37								

The measured values of heat of fusion (ΔH) for the molten salt are listed in Table 3. From the 15 measured data, the mean value of the heat of fusion is 248.32 kJ/kg, which is slightly greater than that of the binary salt of KCl-$MgCl_2$ [29], and is three times as large as that of the ternary chloride molten salt of NaCl-KCl-$ZnCl_2$ [33]. The measurement uncertainty (including systematic and random errors) of the heat of fusion at a 95% confidence interval is ±7.37 (kJ/kg).

3.2 Viscosity. As an important transport property for analysis to heat transfer and pumping power, the dynamic viscosity of the molten salt has been measured with five repetitions in the temperature range of 445 °C to 700 °C. The curves of the viscosity versus temperature from the measurements are shown in Fig. 4. The repeatability of the five tests is acceptable, where the deviation of viscosity values at a temperature is within ±3.5% compared with the average of the five measurements.

The viscosity decreases with the increase of the temperature. With the range of the studied temperatures, the viscosity decreases from 3.85 to 2.5 cP (10^{-3} Pa · s), which is lower than that of the binary chloride salt KCl-$MgCl_2$ (Mole: 68–32%) [29]. Table 4

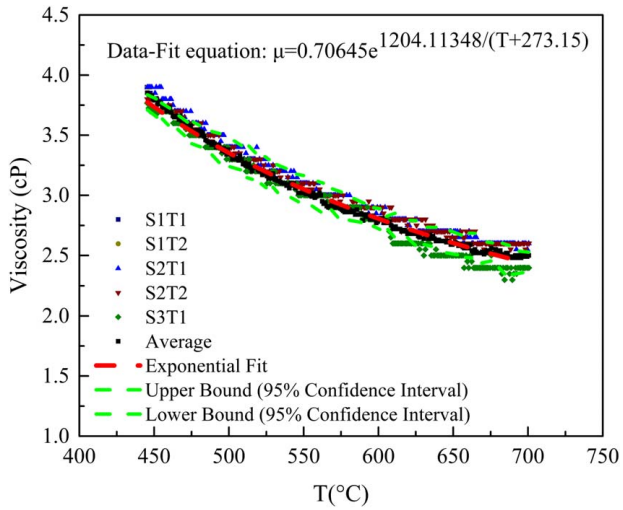

Fig. 4 Comparison of two groups of measured specific heat capacity to theoretical predictions

Table 4 Measured mean values and the overall uncertainties of viscosities at several temperatures

T (°C)	450	500	550	600	650	700
$\bar{\mu}$ (cP)	3.79	3.36	3.03	2.79	2.60	2.5
$u_{\bar{\mu}}$ (cP)	0.0853	0.1066	0.1138	0.0859	0.0872	0.0903

lists the measured mean viscosities and the measurement uncertainty at a probability of 95% at several points of temperatures. The maximum measurement uncertainty is ±0.16 cP, which is ±6.4% relative to the lower viscosities at high temperatures. A regression equation is also shown in Fig. 4, which is to be discussed in the next paragraph.

Viscous flow of substance made of atoms (e.g., molten metals) and simple molecules (molten oxides and molten salts) can usually be approximated by a thermally activated process in classic mechanics. A potential barrier between neighboring atoms needs to be overcome to make the relative motion of atoms, which can be facilitated by high temperature. Therefore, the correlation of viscosity of a temperature dependence of viscous flow and temperature can be expressed by an Arrhenius-type equation [34]

$$\mu = Ae^{B/T} \tag{9}$$

where A is a pre-exponential coefficient and B is the parameter related to the energy barrier to viscous flow with a unit of temperature. It can be rearranged as linear equation by applying natural logarithm on both sides, as shown in Eq. (10)

$$\ln \mu = \ln A + B \times T^{-1} \tag{10}$$

Data regression was conducted for the average value of viscosity (from the five measurements) at each temperature. Figure 5 shows the curve of the natural logarithm of average viscosity ($\ln(\mu)$) versus the inverse of temperature (T^{-1}), where μ and T have the unit of cP and K, respectively. It can be seen that the curve is fairly linear and the coefficient of determination of the regression, R^2, is 0.99128, which is close to 1.0. Therefore, the viscosity of the molten salt indeed follows the thermally activated model and the correlation of μ–T was obtained as:

$$\mu = 0.70645e^{1204.11348/(T+273.15)} \tag{11}$$

where μ has the unit of cP and T is in °C. From the same uncertainty analysis approach shown in Eqs. (7) and (8), the total uncertainty of the regression equations is composed of the uncertainty from the measurement (including system and random errors) and the uncertainty from data fitting. The maximum uncertainty of the regression equation was found to be ±0.1138 cP, while the uncertainty of curve fitting is 0.0036 cP and thus negligible.

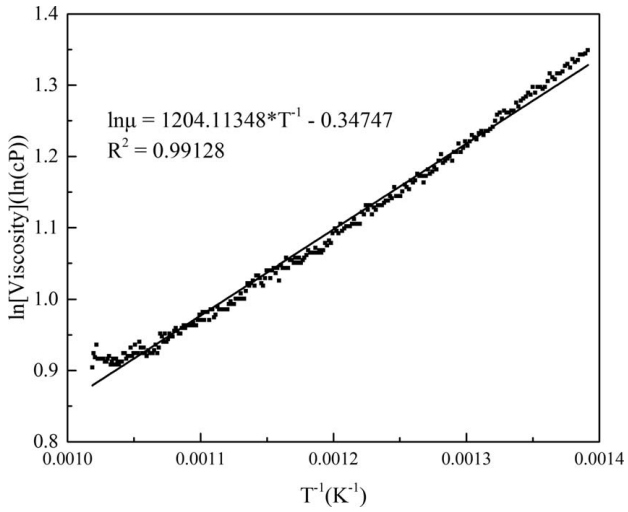

Fig. 5 The linear relationship of ln(μ) versus T^{-1}

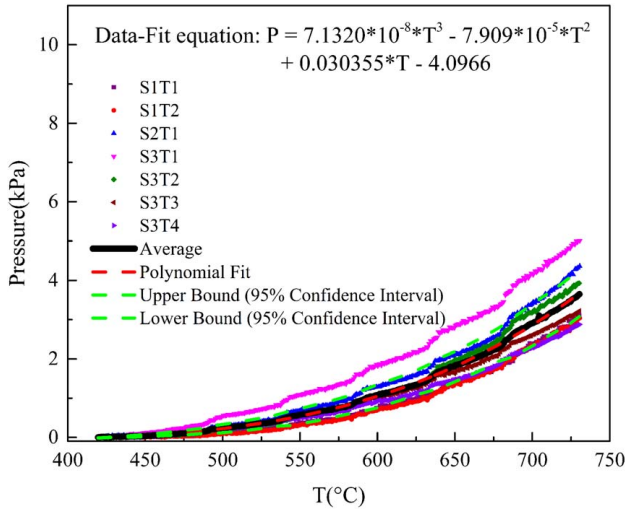

Fig. 6 Measured vapor pressures against temperatures

Table 5 Measured average value and overall uncertainty of vapor pressures at several temperatures

T (°C)	500	550	600	650	700	725
$\bar{P}$ (kPa)	0.247	0.576	1.078	1.825	2.910	3.484
$u_{\bar{P}}$ (kPa)	0.111	0.188	0.281	0.391	0.520	0.589

3.3 Vapor Pressure. Relatively low vapor pressure was observed for the current ternary chloride salt $MgCl_2$-KCl-NaCl. The systematic error of the pressure measurement is ±0.08% of reading. Figure 6 shows the curves of vapor pressure varying against temperatures of the molten salt. There were seven measurements conducted from 420 °C to 725 °C in this experiment, which showed an acceptable repeatability. It is seen that the vapor pressure increases with the increase of temperature greater than linear correlation. The measured average vapor pressure from seven times of tests, and the measurement uncertainty (including systematic error and random error) at a probability of 95% at several temperatures were listed in Table 5. At the temperature of 725 °C, the average measured vapor pressure is 3.5 kPa.

The vapor pressure of the current ternary chloride salt is less than that of binary molten salt KCl-$MgCl_2$ (Mole: 68–32%) [29] and much less than that of ternary molten salt NaCl-KCl-$ZnCl_2$ [33]. The very low vapor pressure of $MgCl_2$ compared with that of $ZnCl_2$ could be the major contribution factor for this low pressure in these two $MgCl_2$ containing salts [28,35,36]. For the average vapor pressures at measured temperatures, a polynomial equation was fitted as given in Eq. (12), where P has a unit of kPa and T is in °C. The uncertainty from curve fitting is 2.8×10^{-3} kPa which is negligible compared with the maximum measurement uncertainty of ±0.589 kPa (including system error of ±0.08% of reading, and random error). Considering the measurement uncertainty in Table 5 and the error from curve fitting, the maximum total uncertainty of the equation for pressure is ±0.589 kPa

$$P = 7.1320 * 10^{-8} \times T^3 - 7.909 \times 10^{-5} \times T^2 + 0.030355 \times T - 4.0966 \tag{12}$$

3.4 Density. The density of the current chloride molten salt has been measured at temperatures ranging from 430 °C to

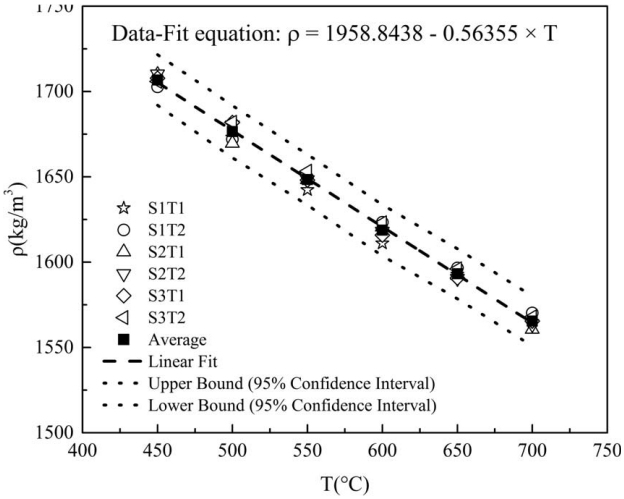

Fig. 7 The molten salt density versus temperature

700 °C, as shown in Fig. 7. The 6 times of measurement showed a very good repeatability and the density linearly decreases with the increase of the temperature. A linear regression was conducted which resulted in Eq. (13), where ρ and T have the unit of kg/m^3 and °C, respectively.

Given in Table 6 are the measured average value of density (due to six tests) and the measurement uncertainty (including systematic and random errors) at a probability of 95% at several points of temperatures. The density of the molten salt decreases from 1706.7 kg/m^3 to 1565.5 kg/m^3 in the temperatures from 450 to 700 °C. The maximum measurement uncertainty is ±15.183 kg/m^3, which is less than 1% of the density. The uncertainty of curve fitting is obtained as ±1.667 kg/m^3 using Eq. (7). Therefore, the total maximum uncertainty for the density from using Eq. (13) is ±15.27 kg/m^3

$$\rho = 1958.8438 - 0.56355 \times T \tag{13}$$

Table 6 Measured average value and overall uncertainty of density

T (°C)	450	500	550	600	650	700
$\bar{\rho}$ (kg/m^3)	1706.7	1676.5	1648.3	1618.7	1593.1	1565.5
$u_{\bar{\rho}}$ (kg/m^3)	14.757	15.183	14.729	14.903	14.502	14.550

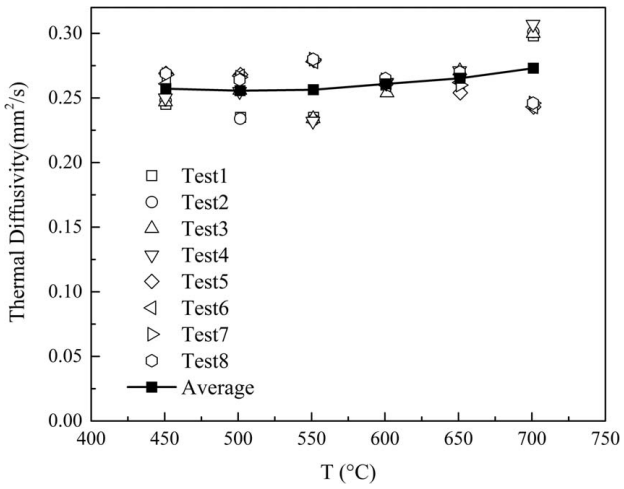

Fig. 8 The measured thermal diffusivity versus temperature

Table 7 Measured average value and the uncertainty at a probability of 95% for thermal diffusivity

T (°C)	450	500	550	600	650	700
$\bar{\alpha}$ (mm^2/s)	0.2571	0.2556	0.2564	0.2609	0.2653	0.2730
$u_{\bar{\alpha}}$ (mm^2/s)	0.0105	0.0121	0.0181	0.0081	0.0089	0.0221

Table 8 Measured average value and overall uncertainty of thermal conductivity

T (°C)	450	500	550	600	650	700
κ (W/m · K)	0.4724	0.4506	0.4337	0.4229	0.4126	0.4066
u_κ (W/m · K)	0.0239	0.0263	0.0344	0.0202	0.0209	0.0364

3.5 Thermal Diffusivity. In order to measure the thermal conductivity of the molten salt, the thermal diffusivity was first measured as described in Sec. 2.5. Figure 8 shows the obtained thermal diffusivity for the current molten salt with a total of eight measurements at a series of temperatures. The mean value and the uncertainty of the measured thermal diffusivity were obtained and listed in Table 7 for several points of temperatures. The measured thermal diffusivity slightly increases with the increase of temperature in the range of 450–700 °C. The maximum uncertainty of measurement (including systematic error of ±3% of reading, and random error) of the measured diffusivity is seen at 700 °C, which is ±0.0221 mm^2/s at a probability of 95%. Data regression analysis for the mean values was conducted and a second-order polynomial correlation (Eq. (14)) could show the best fit for the thermal diffusivity against temperature. In the equation, the diffusivity α has the unit of mm^2/s and temperature T is in °C. The uncertainty of the regression equation is ±0.00076 mm^2/s. Therefore, the maximum uncertainty of using Eq. (14) is ±0.0221 mm^2/s

$$\alpha = 4.338 \times 10^{-7} \times T^2 - 4.353 \times 10^{-4} \times T + 0.365 \tag{14}$$

3.6 Thermal Conductivity. The thermal conductivity (κ) of the molten salt is calculated using Eq. (2) as determined by the three measured independent variables—thermal diffusivity (α), specific heat capacity (C_p), and density (ρ). The uncertainty of thermal conductivity κ is thus derived from Eq. (2), which is expressed as a

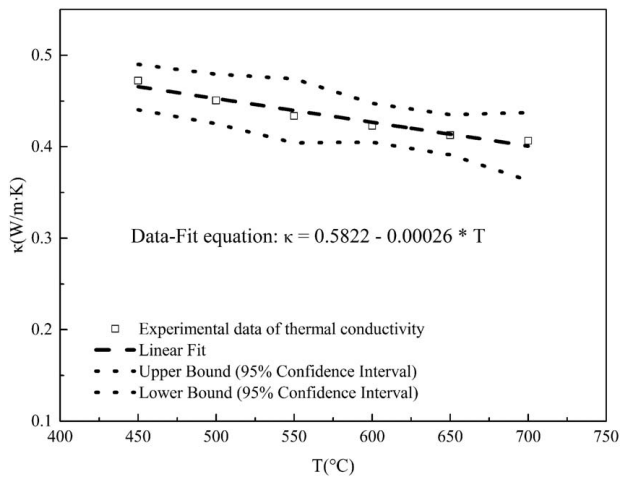

Fig. 9 Thermal conductivity of the molten salt at various temperatures

Table 9 Summary of thermophysical properties of the current molten salt for Gen3 CSP

Property	Values or correlations with T (°C)	Uncertainties @ probability of 95%
Melting point (°C)	401.4	±1.3
Heat of fusion (kJ/kg)	248.32	±7.37
Heat capacity (J/g · K)	$C_p = 1.30138 - 0.0005 * T$	±0.0358
Viscosity (cP or 10^{-3} Pa · s)	$\mu = 0.70645e^{1204.11348/(T+273.15)}$	±0.1138
Vapor pressure (kPa)	$P = 7.1320 \times 10^{-8} \times T^3 - 7.909 \times 10^{-5} \times T^2 + 0.030355 \times T - 4.0966$	±0.589
Density (kg/m^3)	$\rho = 1958.8438 - 0.56355 \times T$	±15.27
Thermal conductivity (W/m · K)	$\kappa = 0.5822 - 2.6 \times 10^{-4} \times T$	±0.037

function of the measured variables α, ρ, and C_p, in Eq. (15)

$$u_\kappa = \sqrt{\left(\frac{\partial \kappa}{\partial \alpha}\right)^2 * u_\alpha^2 + \left(\frac{\partial \kappa}{\partial \rho}\right)^2 * u_\rho^2 + \left(\frac{\partial \kappa}{\partial C_p}\right)^2 * u_{C_p}^2} = \sqrt{(\rho \times C_p \times u_\alpha)^2 + (\alpha \times C_p \times u_\rho)^2 + (\alpha \times \rho \times u_{C_P})^2} \quad (15)$$

For every obtained thermal conductivity, the uncertainty of measurement is calculated and listed in Table 8. A linear regression equation for the thermal conductivity was obtained as given in Eq. (16), which has an uncertainty of ±0.0066 W/m · K from the data fitting with a probability of 95%. The units of thermal conductivity (κ) and temperature T in Eq. (16) are W/m · K and °C, respectively. Therefore, if Eq. (16) is used to calculate the thermal conductivity, the total uncertainty at the measured temperatures is obtained as the root of the sum of squares of the measurement uncertainty and the uncertainty from data fitting. The maximum uncertainty for using Eq. (16) is ±0.037 W/m · K.

Figure 9 shows the measured thermal conductivity values of the molten salt, which range from 0.4724 to 0.4066 W/m · K in the temperature range of 450 °C to 700 °C. The decrease of the thermal conductivity versus the increase of temperature is not very significant in the interested range of temperature. It has been compared that the thermal conductivity of the current ternary chloride salt is close to that of the binary salt KCl-$MgCl_2$ (Mole: 68–32%) [29] but greater than the thermal conductivity of three types of ternary salts by NaCl, KCl, and $ZnCl_2$ as given in literature [33] in the similar temperature range

$$\kappa = 0.5822 - 0.00026 * T \quad (16)$$

Finally, a summary for the measured properties of the current molten salt is given in Table 9. For each property, the maximum overall uncertainty of the value obtained using the corresponding equation is also listed.

It is also very important to mention that all the obtained regression equations for properties have been trialed for extended temperatures up to 800 °C. For every property, the calculated values at temperatures beyond the tested range still follow the variation trend of tested data very well. Therefore, authors are confident that the use of these equations may be extended to the temperature up to 800 °C if needed in engineering application.

4 Conclusion

In this paper, the first comprehensive experimental measurements were conducted to study the thermal and transport properties of a new eutectic chloride molten salt, which is consisted of $MgCl_2$–KCl–NaCl at weight percentages of 45.98–38.91–15.11% correspondingly. The measured properties and their values of range are summarized to serve the need of engineering designs for the third-generation concentrated solar thermal power plants.

(1) The melting point and heat of fusion of the eutectic salt are 401.4 °C and 248.32 kJ/kg, respectively.
(2) The specific heat of the liquid eutectic salt deceases linearly from 1.0904 to 0.9936 J/g · K when the molten salt temperature increases from 450 to 625 °C.
(3) The viscosity of the eutectic liquid salt decreases from 3.79 to 2.5 cP when the molten salt temperature increases from 450 to 700 °C. At temperatures above 550 °C, the molten salt viscosity is below 3 cP.
(4) The vapor pressure of this eutectic molten salt is less than 5 kPa at a temperature as high as 725 °C.
(5) The density of the current eutectic molten salt decrease from 1706.7 kg/m^3 to 1565.5 kg/m^3 when the temperature increase from 450 °C to 700 °C. The density decreases linearly with the increase of temperature.
(6) The thermal conductivity of the eutectic molten salt has been measured through measurement of its thermal diffusivity, specific heat capacity, and density. The thermal conductivity decreases from 0.4724 to 0.4066 W/(m · K) in the temperature range of 450 to 700 °C.

Extrapolation to the property equations was checked that the use of these equations may be extended to the temperature up to 800 °C if needed in engineering application.

Acknowledgment

The authors are grateful that the work was funded by U.S. Department of Energy (DOE) under Contract No. DE-AC36-08GO28308 through National Renewable Energy Laboratory, operated by Alliance for Sustainable Energy, LLC.

Conflict of Interest

There are no conflicts of interest.

References

[1] Pandey, A. K., Hossain, M. S., Tyagi, V. V., Abd Rahim, N., Jeyraj, A., Selvaraj, L., and Sari, A., 2018, "Novel Approaches and Recent Developments on Potential Applications of Phase Change Materials in Solar Energy," Renewable Sustainable Energy Rev., **82**(1), pp. 281–323.
[2] Blaga, R., Sabadus, A., Stefu, N., Dughir, C., Paulescu, M., and Badescu, V., 2019, "A Current Perspective on the Accuracy of Incoming Solar Energy Forecasting," Prog. Energy Combust. Sci., **70**, pp. 119–144.
[3] Indora, S., and Kandpal, T. C., 2018, "Institutional Cooking With Solar Energy: A Review," Renewable Sustainable Energy Rev., **84**, pp. 131–154.
[4] Carrillo, A. J., González-Aguilar, J., Romero, M., and Coronado, J. M., 2019, "Solar Energy on Demand: A Review on High Temperature Thermochemical Heat Storage Systems and Materials," Chem. Rev., **119**(7), pp. 4777–4816.
[5] Solangi, K. H., Islam, M. R., Saidur, R., Rahim, N. A., and Fayaz, H., 2011, "A Review on Global Solar Energy Policy," Renewable Sustainable Energy Rev, **15**(4), pp. 2149–2163.
[6] Sarkodie, S. A., and Strezov, V., 2019, "Effect of Foreign Direct Investments, Economic Development and Energy Consumption on Greenhouse Gas Emissions in Developing Countries," Sci. Total Environ., **646**, pp. 862–871.
[7] Sampaio, P. G. V., and González, M. O. A., 2017, "Photovoltaic Solar Energy: Conceptual Framework," Renewable Sustainable Energy Rev., **74**, pp. 590–601.
[8] Stropnik, R., and Stritih, U., 2016, "Increasing the Efficiency of PV Panel With the Use of PCM," Renewable Energy, **97**, pp. 671–679.
[9] Stoffel, T., Renné, D., and Myers, D., 2010, "Concentrating Solar Power-Best Practices Handbook for the Collection and Use of Solar Resource Data (CSP),"

Technical Report National Renewable Energy Laboratory, **NREL/TP-550-47465**, pp. 1–146.
[10] Seitz, M., Cetin, P., and Eck, M., 2014, "Thermal Storage Concept for Solar Thermal Power Plants With Direct Steam Generation," Energy Procedia, **49**, pp. 993–1002.
[11] Toro, C., Rocco, M., and Colombo, E., 2016, "Exergy and Thermoeconomic Analyses of Central Receiver Concentrated Solar Plants Using Air as Heat Transfer Fluid," Energies, **9**(11), p. 885.
[12] Neises, T., and Turchi, C., 2014, "A Comparison of Supercritical Carbon Dioxide Power Cycle Configurations With an Emphasis on CSP Applications," Energy Procedia, **49**, pp. 1187–1196.
[13] Coco Enríquez, L., Muñoz Antón, J., and Martínez-Val Peñalosa, J. M., 2016, "Comparison Between s-CO_2 and Other Supercritical Working Fluids (s-Ethane, s-SF6, s-Xe, s-CH_4, s-N_2) in Line-Focusing Solar Power Plants with Supercritical Brayton Power Cycles," ECRES 2016 European Conference on Renewable Energy Systems, Istanbul, Turkey, Aug. 28–31.
[14] Eck, M., and Hennecke, K., 2007, "Heat Transfer Fluids for Future Parabolic Trough Solar Thermal Power Plants," Proceedings of ISES Solar World Congress 2007: Solar Energy and Human Settlement, Beijing, China, Sept. 18–21, Vols. I–V, pp. 1806–1812.
[15] Cabaleiro, D., Pastoriza-Gallego, M. J., Piñeiro, M. M., Legido, J. L., and Lugo, L., 2012, "Thermophysical Properties of (Diphenyl Ether + Biphenyl) Mixtures for Their Use as Heat Transfer Fluids," J. Chem. Thermodyn., **50**, pp. 80–88.
[16] Wojcik, J. D., and Wang, J., 2018, "Feasibility Study of Combined Cycle Gas Turbine (CCGT) Power Plant Integration With Adiabatic Compressed Air Energy Storage (ACAES)," Appl. Energy, **221**, pp. 477–489.
[17] Jalili Jamshidian, F., Gorjian, S., and Shafiee Far, M., 2018, "An Overview of Solar Thermal Power Generation Systems," J. Sol. Energy Res., **3**(4), pp. 301–312.
[18] González-Roubaud, E., Pérez-Osorio, D., and Prieto, C., 2017, "Review of Commercial Thermal Energy Storage in Concentrated Solar Power Plants: Steam vs. Molten Salts," Renewable Sustainable Energy Rev., **80**, pp. 133–148.
[19] Liu, Q., and Lange, R. A., 2003, "New Density Measurements on Carbonate Liquids and the Partial Molar Volume of the $CaCO_3$ Component," Contrib. Mineral. Petrol., **146**(3), pp. 370–381.
[20] Olivares, R. I., Chen, C., and Wright, S., 2012, "The Thermal Stability of Molten Lithium–Sodium–Potassium Carbonate and the Influence of Additives on the Melting Point," ASME J. Sol. Energy Eng., **134**(4), p. 041002.
[21] An, X., Cheng, J., Zhang, P., Tang, Z., and Wang, J., 2016, "Determination and Evaluation of the Thermophysical Properties of an Alkali Carbonate Eutectic Molten Salt," Faraday Discuss., **190**, pp. 327–338.
[22] Li, Y., Xu, X., Wang, X., Li, P., Hao, Q., and Xiao, B., 2017, "Survey and Evaluation of Equations for Thermophysical Properties of Binary/Ternary Eutectic Salts From NaCl, KCl, $MgCl_2$, $CaCl_2$, $ZnCl_2$ for Heat Transfer and Thermal Storage Fluids in CSP," Sol. Energy, **152**, pp. 57–79.
[23] Zhao, Y., and Vidal, J., 2020, "Potential Scalability of a Cost-Effective Purification Method for $MgCl_2$-Containing Salts for Next-Generation Concentrating Solar Power Technologies," Sol. Energy Mater. Sol. Cells, **215**, p. 110663.
[24] Xu, X., Dehghani, G., Ning, J., and Li, P., 2018, "Basic Properties of Eutectic Chloride Salts NaCl-KCl-$ZnCl_2$ and NaCl-KCl-$MgCl_2$ as HTFs and Thermal Storage Media Measured Using Simultaneous DSC-TGA," Sol. Energy, **162**, pp. 431–441.
[25] ASTM Standard E1269-11, 2018, "Standard Test Method for Determining Specific Heat Capacity by Differential Scanning Calorimetry," ASTM International, West Conshohocken, PA, www.astm.org, Accessed May 2019.
[26] Rincon, J. D., 2020, "Experimental Measurements for Melting Point, Heat of Fusion and Heat Capacity of Several Eutectic Molten Salts by NaCl-KCl-$MgCl_2$," Master's thesis, Department of Aerospace and Mechanical Engineering, University of Arizona, Spring, Tucson, AZ.
[27] Nitta, K., Nohira, T., Hagiwara, R., Majima, M., and Inazawa, S., 2009, "Physicochemical Properties of $ZnCl_2$–NaCl–KCl Eutectic Melt," Electrochim. Acta, **54**(21), pp. 4898–4902.
[28] Wang, K., Molina, E., Dehghani, G., Xu, B., Li, P., Hao, Q., Lucas, P., Kassaee, M. H., Jeter, S. M., and Teja, A. S., 2014, "Experimental Investigation to the Properties of Eutectic Salts by NaCl-KCl-$ZnCl_2$ for Application as High Temperature Heat Transfer Fluids," ASME 2014 8th International Conference on Energy Sustainability Collocated with the ASME 2014 12th International Conference on Fuel Cell Science, Engineering and Technology, Boston, MA, June 30–July 2, American Society of Mechanical Engineers Digital Collection.
[29] Xu, X., Wang, X., Li, P., Li, Y., Hao, Q., Xiao, B., Elsentriecy, H., and Gervasio, D., 2018, "Experimental Test of Properties of KCl–$MgCl_2$ Eutectic Molten Salt for Heat Transfer and Thermal Storage Fluid in Concentrated Solar Power Systems," ASME J. Sol. Energy Eng., **140**(5), p. 051011.
[30] Segal, E., 2015, "Density Measurement and Modeling of Eutectic Molten Salts," Master's thesis, Department of Aerospace and Mechanical Engineering, University of Arizona, Tucson, AZ.
[31] Bale, C. W., Bélisle, E., Chartrand, P., Decterov, S. A., Eriksson, G., Gheribi, A. E., Hack, K., Jung, I. H., Kang, Y. B., Melançon, J., Pelton, A. D., Petersen, S., Robelin, C., Sangster, J., Spencer, P., and Van Ende, M. A., 2016, "FactSage Thermochemical Software and Databases, 2010–2016," Calphad, **54**, pp. 35–53.
[32] FactSage Software package, http://www.factsage.com/
[33] Li, P., Molina, E., Wang, K., Xu, X., Dehghani, G., Kohli, A., Hao, Q., Kassaee, M. H., Jeter, S. M., and Teja, A. S., 2016, "Thermal and Transport Properties of NaCl–KCl–$ZnCl_2$ Eutectic Salts for New Generation High-Temperature Heat-Transfer Fluids," ASME J. Sol. Energy Eng., **138**(5), p. 054501.
[34] Messaâdi, A., Dhouibi, N., Hamda, H., Belgacem, F. B. M., Adbelkader, Y. H., Ouerfelli, N., and Hamzaoui, A. H., 2015, "A New Equation Relating the Viscosity Arrhenius Temperature and the Activation Energy for Some Newtonian Classical Solvents," J Chem., **2015**(12), p. 163262.
[35] Keneshea, F., and Cubicciotti, D., 1964, "Vapor Pressures of Zinc Chloride and Zinc Bromide and Their Gaseous Dimerization," J. Chem. Phys., **40**(1), pp. 191–199.
[36] Mohan, G., Venkataraman, M., Gomez-Vidal, J., and Coventry, J., 2018, "Assessment of a Novel Ternary Eutectic Chloride Salt for Next Generation High-Temperature Sensible Heat Storage," Energy Convers. Manage., **167**, pp. 156–164.